

# Reconstitution of functionalized transmembrane domains of receptor proteins into bio-mimetic membranes

*Daniel R. Scott<sup>†Δ\*</sup>, Vitalii Silin<sup>Δ</sup>, and Hirsh Nanda<sup>†°</sup>*

<sup>†</sup>Center for Neutron Research, National Institute of Standards and Technology, Gaithersburg, Maryland 20899, United States

<sup>Δ</sup>Institute of Bioscience and Biotechnology Research (University of Maryland), Rockville, Maryland 20850, United States

## *Supplemental Methods*

### Peptide Synthesis:

Each peptide was functionalized with an N-terminus biotin moiety for streptavidin ligation studies, while the C-terminus was amidated to reduce charge and mimic the peptide's native sequence. Two additional residues on each side of the defined TM domain were retained to conserve sequence identity, as to promote native folding of the peptide within a membrane environment. A native cysteine residue was changed to serine (in bold) to avoid disulfide cross-

linking, and the internal tryptophan (underlined, in bold) replaced a native phenylalanine residue within the TM domain for fluorescence studies. Finally, a total of nine lysines capping either end of the sequence were deemed appropriate to offset the TM core hydrophobicity and improve water solubility, an adopted method outlined in Cunningham *et al.*, 2007.<sup>1</sup>

Stock solutions of the peptides were made by dissolving the lyophilized powder in ultrapure water (Barnstead NanoPure, Thermo Fisher Scientific Inc.; Waltham, MA). Concentrations were determined from A<sub>280</sub> readings using a NanoDrop 2000 (Thermo Fisher Scientific Inc.; Waltham, MA), as a function of the tryptophan residue.

#### Circular Dichroism:

While several well-established algorithms are offered by the DICHROWEB online server for fitting the data to reference sets of proteins with known secondary structure, applying the CDSSTR algorithm<sup>2,3</sup> to the data produced the lowest and most consistent normalized root mean square deviation (NRMSD) values and, thus, was adopted here. In addition, the reference set SMP180, designed specifically for membrane protein structure determination,<sup>4</sup> was applied in the secondary structure calculation against the experimental data. It should be noted that changing to another algorithm (CONTINLL<sup>5</sup>) and reference set<sup>6</sup> had minimal impact in the assessment of  $\alpha$ -helix content of the peptides (based on 91 % and 97 % correlations in their secondary structure values, respectively). Another method for calculating  $\alpha$ -helix content (based on the CD spectra's value at  $\theta_{208}$ ) also proved the CDSSTR/SMP180 reliable (91 % correlation).

#### Surface Plasmon Resonance:

Substrates for tandem EIS/SPR (Sapphire chips from Rubicon Technologies, Inc.; Chicago, IL) were vigorously cleaned by piranha solution (a mixture of sulfuric acid and 30 % hydrogen peroxide at volumetric ratios of 7:3) for 30 minutes, then rinsed with ultrapure water and dried

with a nitrogen gas stream. Metal deposition of  $\approx 15 \text{ \AA}$  Cr and  $\approx 400 \text{ \AA}$  Au was performed in a high-energy magnetron (Denton Vacuum Discovery 550) available at the NIST Center for Nanoscale Science and Technology, Nano-Fabrication facility (Gaithersburg, MD). Substrates were then immediately soaked for 8 to 12 hours in ethanol solutions of  $60 \text{ }\mu\text{M}$  HC18 [Z-20-(Z-octadec-9-enyloxy)-3,6,9,12,15,18,22-heptaoxatetracont-31-ene-1-thiol] tethering molecules<sup>7</sup> and  $140 \text{ }\mu\text{M}$   $\beta$ -mercaptoethanol ( $\beta$ ME) – a space-filling component added to co-adsorb to the gold and laterally dilute the HC18 tether – to create a self-assembled monolayer (SAM) with a molar ratio of 7:3  $\beta$ ME:HC18. After rinsing extensively with anhydrous grade ethanol to remove excess soaking solution components, the substrates were dried by nitrogen and mounted onto the SPR instrument. A 1 mL sample chamber was created by clamping a cylindrical teflon tube with a fitted O-ring flush against the Au/SAM surface. All subsequent buffer and sample changes during the SPR experiments were carried out by pipetting.

The SPR instrument utilizes an  $\text{Al}_2\text{O}_3$  (sapphire) prism with a refractive index of 1.77 to facilitate SP excitation even when working with complex high refractive index buffers. Sensitivity by refractive index is better than  $3 \times 10^{-7}$ , approximately an order of magnitude better than the sensitivity of most available commercial devices.

Calibration of SPR was carried out using glycerol and ethylene glycol (EG) solutions. Refractive indexes of water, glycerol and EG are well known and were obtained from the CRC Handbook of Chemistry and Physics (CRC Press; London, UK). Starting concentrations of the solutions were a mass fraction of 20 % glycerol or EG; 1 mL of the solution was added to the SPR cell and the SPR signal was measured. Then 0.25 mL of the solution was removed from the cell and substituted with water; the SPR signal was detected after mixing was completed. This dilution procedure was repeated 5 times. Then dilution was conducted with 0.5 mL water

substitutions until no changes in the SPR signal was detected. This procedure was conducted two times with EG and once with glycerol. The calculated SPR minima shift (by angle) versus refractive index was compared with experimental data refractive index of the solutions versus pixel shift, and the calibration of the angle (in degrees) for one pixel was determined as equal to 0.00008 degrees. Then the calculated dependence of the SPR minimum angle shift versus thickness for a 1.45 refractive index was compared with pixels, assuming the angle/pixel relation obtained from the experiment.

EIS measurements scanned frequencies between 1 Hz and 100 kHz (consisting of 10 logarithmically distributed measurement points per decade), with 10 mV alternating current at 0 V bias versus the reference electrode. The counter electrode was a 0.25 mm diameter platinum wire (99.99% purity; Sigma Aldrich) coiled around the barrel of the reference electrode, and the working electrode was connected to the gold surface by copper conducting tape with single-sided adhesive (SPI Supplies/Structure Probe, Inc.; West Chester, PA). Any derived EIS data were normalized to the working surface area  $A_{el} \approx 0.28 \text{ cm}^2$  exposed to the solution.

Fitting of the EIS data was performed using the ZView software (Scribner Associates, Southern Pines, NC), applying equivalent circuits models (Figure S2) to derive capacitance and resistivity values – as a means to assess bilayer formation in the SPR experiments. The capacitances of the tBLMs and SAM surfaces are evaluated in terms of experimental constant-phase element coefficients (CPE), which are equivalent to capacitance when the  $\alpha_{tBLM}$  exponent value derived in the model approaches 1.0 (our experimental results produced exponents  $\alpha_{tBLM} \geq 0.98$ , considered to reflect near-ideal capacitive behavior<sup>8</sup>). The resistances of the bilayers are also derived from the circuit models, as a parameter quantifying the level of defects in the

tBLMs ( $R_{\text{defect}}$ ). Meanwhile, information can be gleaned from the length of the low-frequency tails in the capacitance plots.

EI measurements of the HC18-anchored POPC lipid bilayers produced high-frequency, semicircular capacitance spectra (Figure S1), similar in shape and amplitude to those reported in Budvytyte *et al.*, 2013, for bilayers tethered to an equivalent SAM composition of 30 % HC18. Additionally, capacitance values of tBLMs derived from the equivalent circuit (Model A) range from 0.92 to 1.04  $\mu\text{F}/\text{cm}^2$  (Table S1), indicating only relatively small deviations in the integrity of the bilayers as they were sequentially treated with peptide and streptavidin. To put these deviations in context, removal of the three peptide-treated bilayers produced near-order-of-magnitude increases in capacitance for each of the three independent surfaces (Table S1). Meanwhile, visual inspection of the low-frequency tails of the capacitance plots indicated that the resistances of the membrane surfaces were not affected by the additions of protein. No decreases in  $R_{\text{defect}}$  values were calculated for the tBLMs following TM peptide incubations, which would have suggested pore formation or an increase in bilayer defects. The overall reproducibility of our results across the multiple bilayer preparations, and in close comparison to data from relevant literature,<sup>7,8</sup> provided confidence in the integrity of the formed bilayers, and deemed the SAM-tBLM surfaces suitable for our concurrent SPR measurements.

#### Neutron Reflectivity Measurements:

Surfaces were cleaned in an aqueous Hellmanex solution at a volume fraction of 5 % and thorough rinsing with ultrapure water (Millipore) and then 99.8 % ethanol and dried in a nitrogen gas stream. Metal deposition of Cr ( $\approx 20 \text{ \AA}$ ) and Au ( $\approx 150 \text{ \AA}$ ) and subsequent SAM formation was performed as stated for the SPR/EIS substrates.

Resolving the structure of protein-membrane complexes by NR requires both proper experimental design and sophisticated data analysis methods. In particular using multiple solvent contrasts (i.e same buffer conditions prepared with 100% H<sub>2</sub>O, 100% D<sub>2</sub>O and a 66% D<sub>2</sub>O, 33% H<sub>2</sub>O mixture) and modeling changes in the reflectivity spectra during each step of the experiment. Therefore surface capture of SA was performed in stages, 1<sup>st</sup> forming a complete tBLM layer, 2<sup>nd</sup> introduction and spontaneous insertion of the TM peptide into the tBLM layer and 3<sup>rd</sup> specific binding of SA to the biotin moiety attached to the inserted TM peptides. At each step the system was measured for  $\approx$  6 hours per isotopic solvent contrasts, providing sufficient counting statistics to resolve signal over background counts with counting times weighted towards the high q region of the scans. Figure S4 shows the reflectivity spectra for each buffer contrast for the different stages of the tBLM (A. neat tBLM preparation; B. EGFR TM peptide insertion; C. SA incubation). Residual differences between the original neat tBLM and their subsequent treatments with protein are shown in the panels below each data set.

Each contrast provides a unique reflectivity spectrum that still reports on the same underlying molecular architecture of the membrane and protein complex. Data was analyzed by fitting an area-fraction distribution of substrate, membrane and protein layers along the z-axis. A composition space model that represents the lipid membrane in terms of overlapping distributions of the different molecular groups (lipid chain, headgroup and tether) was used to represent the tBLM.<sup>9</sup> A Hermite spline was used to model the distribution of the protein along the z-axis without any assumptions of the protein profile. The protein profile was allowed to partially or fully overlap with the membrane where membrane volume was removed proportionally to satisfy a constraint of constant volume filling. The component volume occupancy distribution provides a molecular configuration that is consistent with the data from

multiple solvent contrasts and makes efficient use of the known molecular volumes and geometric constraints in the interfacial structure of the system. Substrate parameters (SiO<sub>x</sub>, Cr & Au) as well as the tether layer were conserved in the model while simultaneously fitting all nine separate data sets. Lipid thickness and the protein profile were allowed to vary between experimental conditions.

## REFERENCES

- (1) Cunningham, F.; Deber, C. M. Optimizing Synthesis and Expression of Transmembrane Peptides and Proteins. *Methods San Diego Calif* **2007**, *41* (4), 370–380.
- (2) Compton, L. A.; Johnson, W. C. Analysis of Protein Circular Dichroism Spectra for Secondary Structure Using a Simple Matrix Multiplication. *Anal. Biochem.* **1986**, *155* (1), 155–167.
- (3) Johnson, W. C. Analyzing Protein Circular Dichroism Spectra for Accurate Secondary Structures. *Proteins* **1999**, *35* (3), 307–312.
- (4) Abdul-Gader, A.; Miles, A. J.; Wallace, B. A. A Reference Dataset for the Analyses of Membrane Protein Secondary Structures and Transmembrane Residues Using Circular Dichroism Spectroscopy. *Bioinforma. Oxf. Engl.* **2011**, *27* (12), 1630–1636.
- (5) Van Stokkum, I. H.; Spoelder, H. J.; Bloemendal, M.; van Grondelle, R.; Groen, F. C. Estimation of Protein Secondary Structure and Error Analysis from Circular Dichroism Spectra. *Anal. Biochem.* **1990**, *191* (1), 110–118.
- (6) Sreerama, N.; Woody, R. W. Estimation of Protein Secondary Structure from Circular Dichroism Spectra: Comparison of CONTIN, SELCON, and CDSSTR Methods with an Expanded Reference Set. *Anal. Biochem.* **2000**, *287* (2), 252–260.
- (7) Budvytyte, R.; Valincius, G.; Niaura, G.; Voiciuk, V.; Mickevicius, M.; Chapman, H.; Goh, H.-Z.; Shekhar, P.; Heinrich, F.; Shenoy, S.; et al. Structure and Properties of Tethered Bilayer Lipid Membranes with Unsaturated Anchor Molecules. *Langmuir ACS J. Surf. Colloids* **2013**, *29* (27), 8645–8656.
- (8) McGillivray, D. J.; Valincius, G.; Vanderah, D. J.; Febo-Ayala, W.; Woodward, J. T.; Heinrich, F.; Kasianowicz, J. J.; Lösche, M. Molecular-Scale Structural and Functional Characterization of Sparsely Tethered Bilayer Lipid Membranes. *Biointerphases* **2007**, *2* (1), 21–33.
- (9) Shekhar, P.; Nanda, H.; Lösche, M.; Heinrich, F. Continuous Distribution Model for the Investigation of Complex Molecular Architectures near Interfaces with Scattering Techniques. *J. Appl. Phys.* **2011**, *110* (10), 102216–10221612.

Supplemental Figures

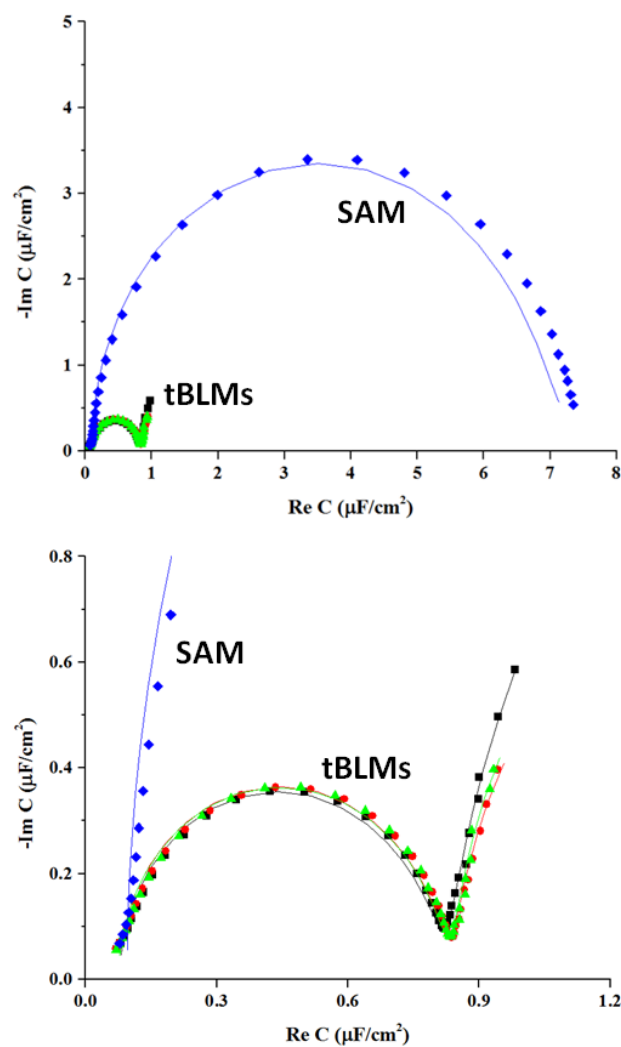


**Figure S1.** Representative EIS complex capacitance plots during SPR measurements: before (■) and after (●) the three independent peptides were incubated with the POPC tBLM, and after streptavidin protein incubation (▲) for each peptide-treated surface. A higher-capacitance plot for the SAM-only surface (30 % HC18; blue diamonds) was also recorded. Corresponding fits of the data are shown as lines, with certain electrical parameters reported in Table S1. The lower panel is a zoom-in of the higher-frequency semicircular plots of the tBLMs.

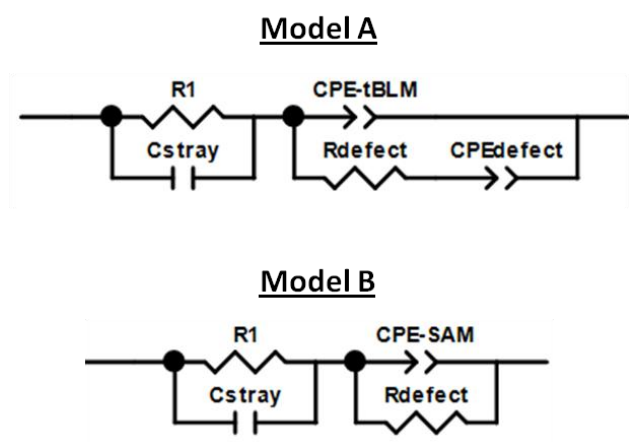


**Figure S2.** Equivalent circuit models used for fitting the EIS data, adopted from Ref. 8. Model A best describes the tethered BLMs, while Model B is suited for the SAM-only surface.

**Table S1. Electrochemical Parameters for SAMs and tBLMs for *in situ* Measurements During SPR Experiments**

	CD4 TM		EGFR TM		E <sub>3a</sub>	
	CPE / μF·cm <sup>-2</sup>	R <sub>defect</sub> / kΩ·cm <sup>2</sup>	CPE / μF·cm <sup>-2</sup>	R <sub>defect</sub> / kΩ·cm <sup>2</sup>	CPE / μF·cm <sup>-2</sup>	R <sub>defect</sub> / kΩ·cm <sup>2</sup>
<i>tBLM</i> <sup>a</sup>	1.04 (0.02)	8.0 (0.5)	0.95 (0.02)	12.9 (1.0)	0.98 (0.03)	13.0 (1.4)
+ <i>Peptide</i> <sup>a</sup>	0.95 (0.02)	16.3 (1.9)	0.93 (0.02)	19.5 (1.4)	0.99 (0.02)	13.7 (1.0)
+ <i>Streptavidin</i> <sup>a</sup>	1.00 (0.02)	16.0 (1.1)	0.92 (0.02)	19.7 (1.3)	0.96 (0.02)	8.3 (0.5)
<i>SAM only</i> <sup>b</sup>	7.96 (0.22)	N/A	10.36 (0.39)	N/A	8.54 (0.26)	N/A

CPE and R<sub>defect</sub> values for the tBLMs and SAM surfaces, as calculated using the appropriate equivalent circuit model (<sup>a</sup>A or <sup>b</sup>B), with standard error values from the fits provided in parentheses. R<sub>defect</sub> values for the SAM surfaces would not converge < 10<sup>14</sup> kΩ·cm<sup>2</sup>, and are therefore listed as “N/A”.

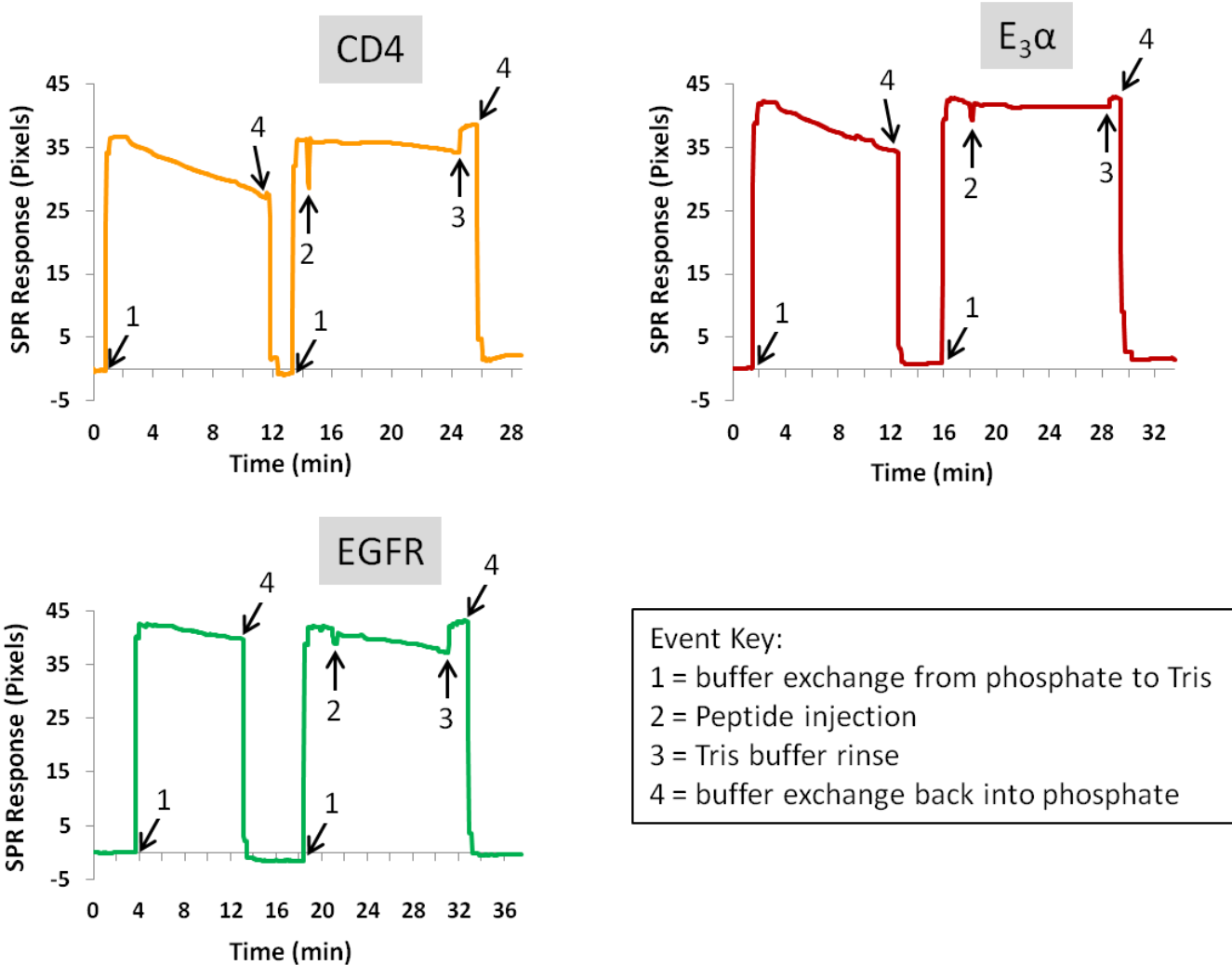


**Figure S3.** SPR sensorgrams for peptide association to POPC bilayers; time-dependent traces recorded on three independent SPR/EIS substrates. Initial jumps in pixel change values ( $\Delta \approx 40$  RUs) correspond to bulk refractive index changes when 10 % acetonitrile in the Tris buffer (10 mM Tris-HCl, 10 mM NaCl, pH 7.2 with 10 % acetonitrile) is exchanged for phosphate buffer (10 mM Na<sub>2</sub>HPO<sub>4</sub>, 100 mM NaCl, pH 7.3). Next, the peptide association of 5  $\mu$ M EGFR, CD4, and E<sub>3</sub>α (in Tris buffer with 10 % acetonitrile) with tethered planar bilayers of POPC lipids. Correspondingly, final pixel change values reflect bilayers incubated back into phosphate buffer for subsequent streptavidin binding.

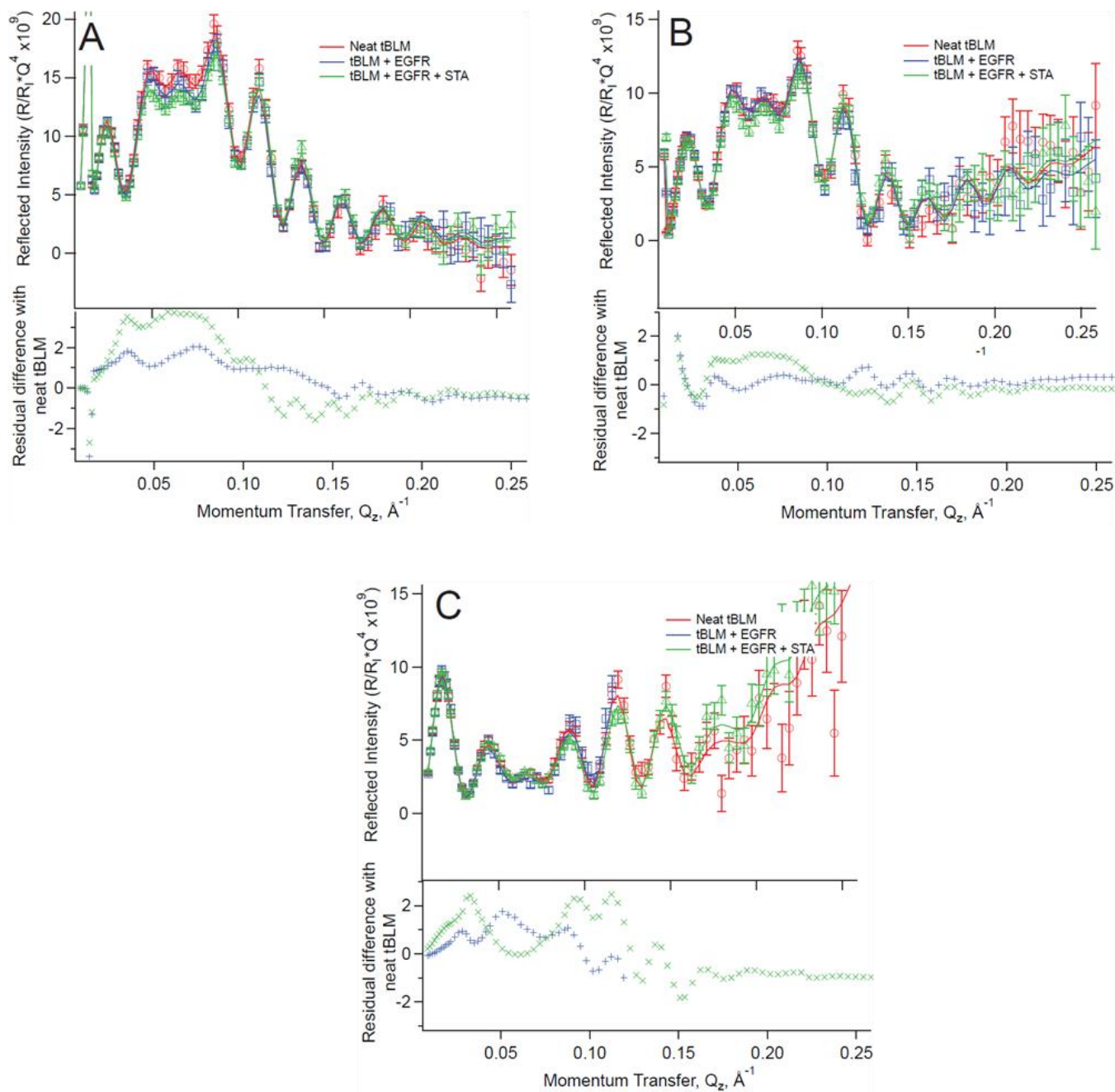


**Figure S4.** Reflectivity data used to elucidate the structural dimensions of the EGFR TM peptide and streptavidin (STA) relative to a tethered membrane. Spectra for all three buffer contrast conditions (A) D<sub>2</sub>O, (B) CM4, and (C) H<sub>2</sub>O solvent are shown. Residuals illustrate the variation in the spectra with the serial additions of the EGFR TM peptide and the streptavidin. Fitting of these data with area fraction distribution models result in the 1-D profiles depicted in Figure 4.